Science Advances

AAAS

advances.sciencemag.org/cgi/content/full/3/11/e1701216/DC1

Supplementary Materials for

Mesocrystalline calcium silicate hydrate: A bioinspired route toward elastic concrete materials

Andreas Picker, Luc Nicoleau, Zaklina Burghard, Joachim Bill, Igor Zlotnikov, Christophe Labbez, André Nonat, Helmut Cölfen

Published 29 November 2017, *Sci. Adv.* **3**, e1701216 (2017)
DOI: 10.1126/sciadv.1701216

The PDF file includes:

- table S1. Mechanical properties of nacre and typical nacre-like layered nanocomposites.
- table S2. Colloidal stability of C-S-H in the presence of different copolymers at various conditions.
- fig. S1. Chemical structures of C-S-H stabilizing polymers.
- fig. S2. AUC measurements of PVP-co-PAA–stabilized C-S-H nanoplates.
- fig. S3. Strategy for the formation of nanostructured hybrid C-S-H.
- fig. S4. Dynamic light scattering of growing C-S-H mesocrystals.
- fig. S5. Evaluation of the mesocrystalline domain sizes of self-assembled C-S-H crystals (approach A).
- fig. S6. Wide-angle x-ray pattern of filtered polymer-stabilized C-S-H nanoplates (red curve) and obtained mesocrystals from pH increase (approach A, black curve) compared to C-S-H from pozzolanic reaction with CaO and SiO2 (Ca/Si = 1) (green curve).
- fig. S7. Thermogravimetric analysis of C-S-H mesocrystals.
- fig. S8. Schematical illustration of the two differently performed nanoindentation experiments on C-S-H mesocrystals from approach A.
- fig. S9. Ashby plot comparing the mechanical properties of the C-S-H mesocrystals (approach A) with various materials.
- fig. S10. SEM images of a cantilever beam used in the bending tests with the applied load perpendicular to the crystal layer planes.
- fig. S11. Schematic illustration of in-situ bending experiments.
- fig. S12. Dimensions of a cantilever beam used in the bending tests with the load applied perpendicular to the crystal layers.

- fig. S13. SEM images of a cantilever beam used in the bending tests with the load applied parallel to the crystal layers.
- Legends for movies S1 and S2
- References (*37*–*49*)

Other Supplementary Material for this manuscript includes the following:
(available at advances.sciencemag.org/cgi/content/full/3/11/e1701216/DC1)

- movie S1 (.mp4 format). Bending test of mesocrystals obtained from pH increase to pH 12.8 under the scanning electron microscope.
  movie S2 (.mp4 format). Bending test of the same mesocrystals such as in movie S1 except that the applied stress is parallel to the crystal layer planes.

table S1. Mechanical properties of nacre and typical nacre-like layered nanocomposites. MTM stands for Montmorillonite, PDDA for poly(diallyldimethylammonium chloride), PVA for poly(vinyl alcohol), PE for polyelectrolyte, CMC for carboxymethyl cellulose, SA for self assembling, LCST for liquid crystal self-templating, GGO for Giant Graphene oxide and HPG for hyperbranched polyglycerol.

Nacre like layered nano composite	Synthesis approach	Inorganic fraction (^{vol}%)	Young's modulus (GPa)	Tensile strength (MPa)	Bending strength (MPa)	Year, ref
Nacre	Biomineralization	95	60-70	140-180	210 (2)	1994 *(37)*, 2001 *(25)*
MTM/PDDA	LBL	30	11±2	106 ± 11		2003 *(38)*
MTM/ Chitosan	LBL	42	6.1 ± 0.8	81 ± 12		2007 *(39)*
MTM/PVA	LBL	50	13±2	150±40		2007 *(40)*
MTM/PVA +GA	LBL	50	106±11	400±40		2007 *(40)*
MTM/PVA +Cu^{2+}	LBL	50	58±6	320±40		2008 *(41)*
MTM/PVA +Al^{3+}	LBL	50	41±5	250±50		2008 *(41)*
Gibbsite/Silane	Electrophoretic deposition	50	5.4	55		2009 *(42)*
Alumina/PMMA	LBL	80	115		210	2008 *(43)*
MTM/Chitosan	SA	70	6.8 ±1.6	99 ±13		2010 *(44)*
$CaCO_3$/PE	LBL	50	38			2012 *(45)*
$(MTM/PDDA)_{100salt}$	LBL	50	9.4±2.4			2013 *(46)*
MTM /CMC	SA	80	16.6±3.6	142 ± 10		2013 *(47)*
GGO/HPG-GA	Wet Spinning	77	20.9	652		2013 *(48)*

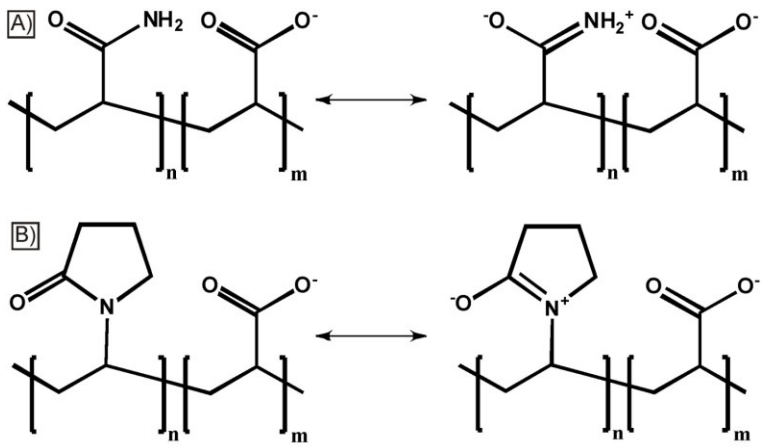

fig. S1. Chemical structures of C-S-H stabilizing polymers. (A) PAAm-co-PAA and **(B)** PVP-co-PAA with their resonance structures

table S2. Colloidal stability of C-S-H in the presence of different copolymers at various conditions.

Polymer	pH	Concentration [g/l]	Duration of Stabilization
PAAm-co-PAA 200000	12	0.1	one day
	12	1.0	several months
	13	1.0	immediate agglomeration
PAAm-co-PAA 520000	12	0.1	some days
	12	1.0	several months
	13	1.0	immediate agglomeration
PVP-co-PAA 96000	12	0.1	few hours
	12	1.0	several months
	13	1.0	immediate agglomeration

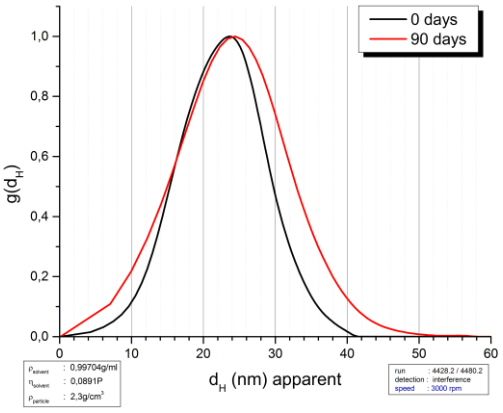

fig. S2. AUC measurements of PVP-co-PAA–stabilized C-S-H nanoplates. The particle size distributions do not change much over a period of 90 days confirming the given colloidal stability of the C-S-H dispersion.

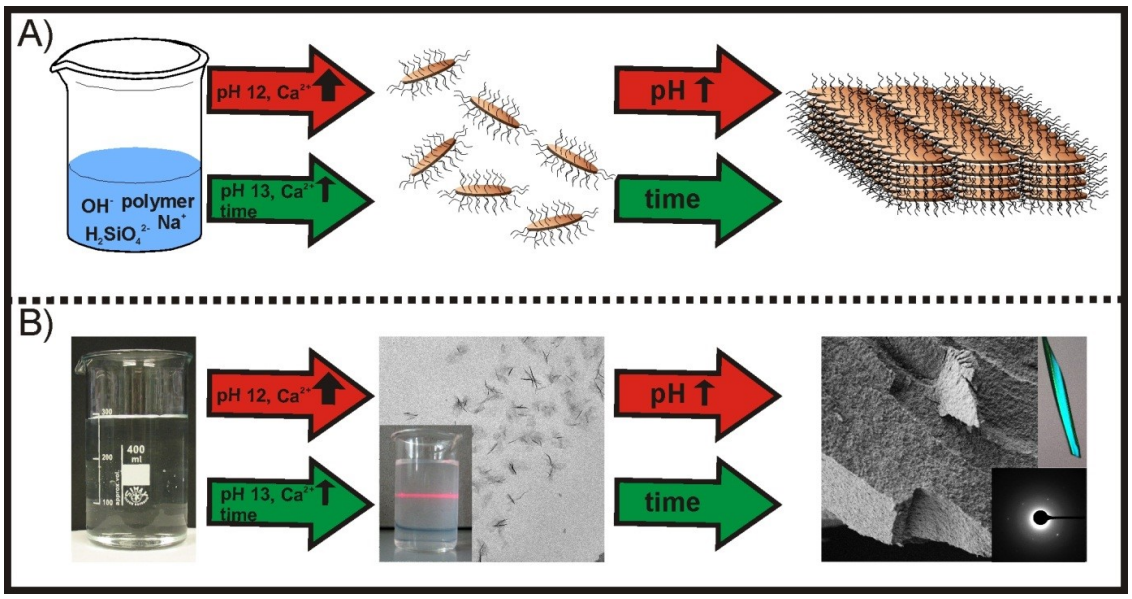

fig. S3. Strategy for the formation of nanostructured hybrid C-S-H. (A) Schematical representation, **(B)** real outcome. Red arrows indicate the pathway via pH increase (approach A), green arrows the C-S-H/polymer ratio pathway at pH 13 (approach B). **Red:** Colloidal C-S-H is synthesized in presence of stabilizing polymers by titrating $CaCl_2$ into Na_2SiO_3 at pH 12 until nucleation occurs. Subsequent pH increase triggers the self-assembly of crystallites to mesocrystals. **Green:** The Na_2SiO_3/polymer solution is supersaturated with calcium at pH 13 without triggering immediate nucleation. With an exactly defined supersaturation the amount of precipitating C-S-H and thus the C-S-H/polymer ratio is adjusted. Here, C-S-H mesocrystals form in a one-pot reaction. First, polymer-stabilized crystallites nucleate after a while before they self-assemble with time. Superstructures from both approaches show layered structures as well as long-range orientation over several hundreds of micrometers and a perfect mutual alignment in three dimensions with domain sizes around 1 μm^2. Due to their incorporated organic content ranging between 5 – 20 wt.% they show a highly-enhanced elasticity compared to C-S-H in real cementitious systems.

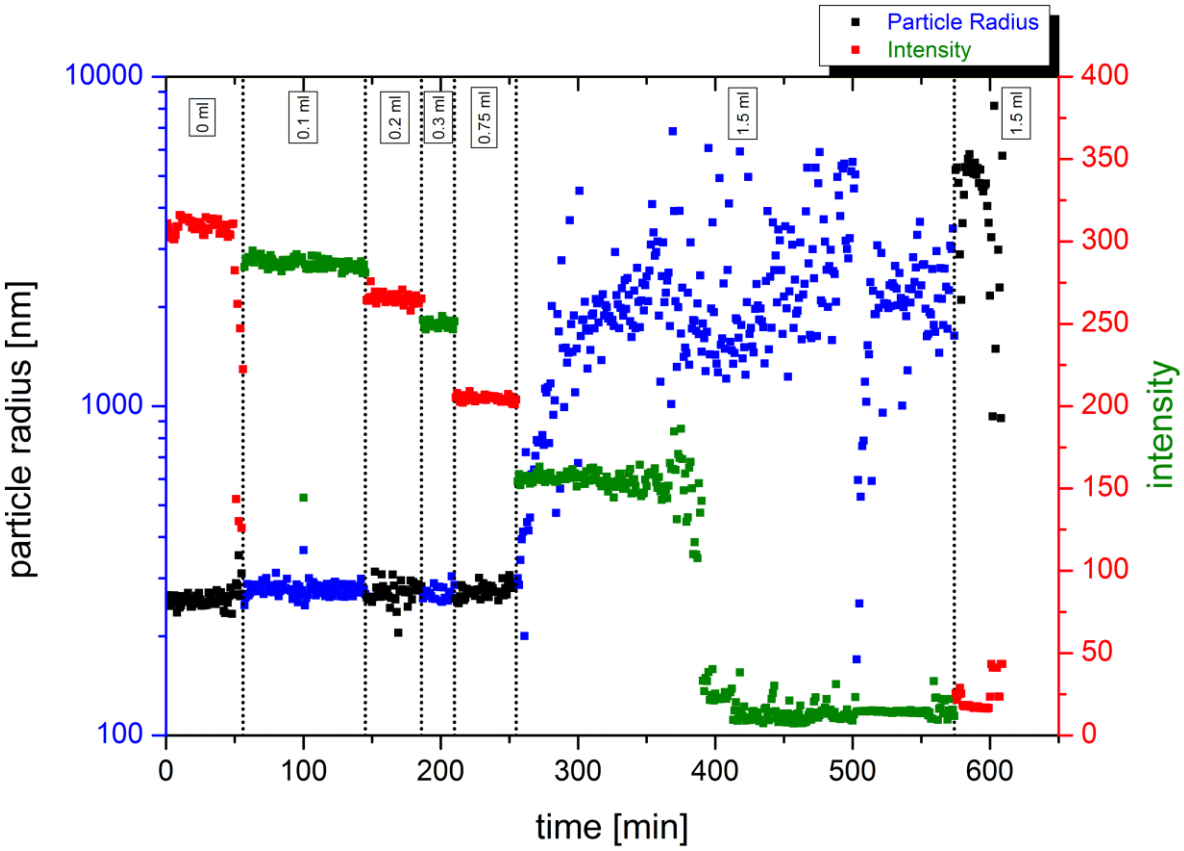

fig. S4. Dynamic light scattering of growing C-S-H mesocrystals. Time resolved dynamic light scattering investigation of C-S-H mesocrystal formation after a pH increase according to approach (A). A C-S-H solution was prepared with PAAm-co-PAA 520000 as stabilizing agent. 2 ml of this solution were then laced with different aliquots of 1 M NaOH until the agglomeration of the C-S-H plates was observed. Every 60 seconds, a new measurement was launched in an endless loop. The corresponding measurements after the total addition of 0.1 ml, 0.2 ml, 0.3 ml, 0.75 ml and 1.5 ml 1 M NaOH are shown in the figure.

At the beginning, the particle radius stays rather constant and only the intensity is decreased due to the dilution effect. Then, 2 minutes after the total addition of 1.5 ml NaOH the agglomeration of the C-S-H particles starts. As it can be seen, it takes roughly one hour until the final size of the C-S-H mesocrystals in solution is reached. From the constant intensity value between 260 and 360 minutes it can be deduced, that agglomerated particles stay stable in solution. Only 1.5 hours after the NaOH triggered agglomeration, the C-S-H particles aggregate to bigger structures which are then sedimenting upon further growth (indicated by the intensity decrease and the huge fluctuation in the size signal around 360 minutes). This experiment suggests that the agglomeration process is taking place not at once as it is the case in absence of stabilizing agents but rather occurs via a particle attachment mechanism over a longer period of time.

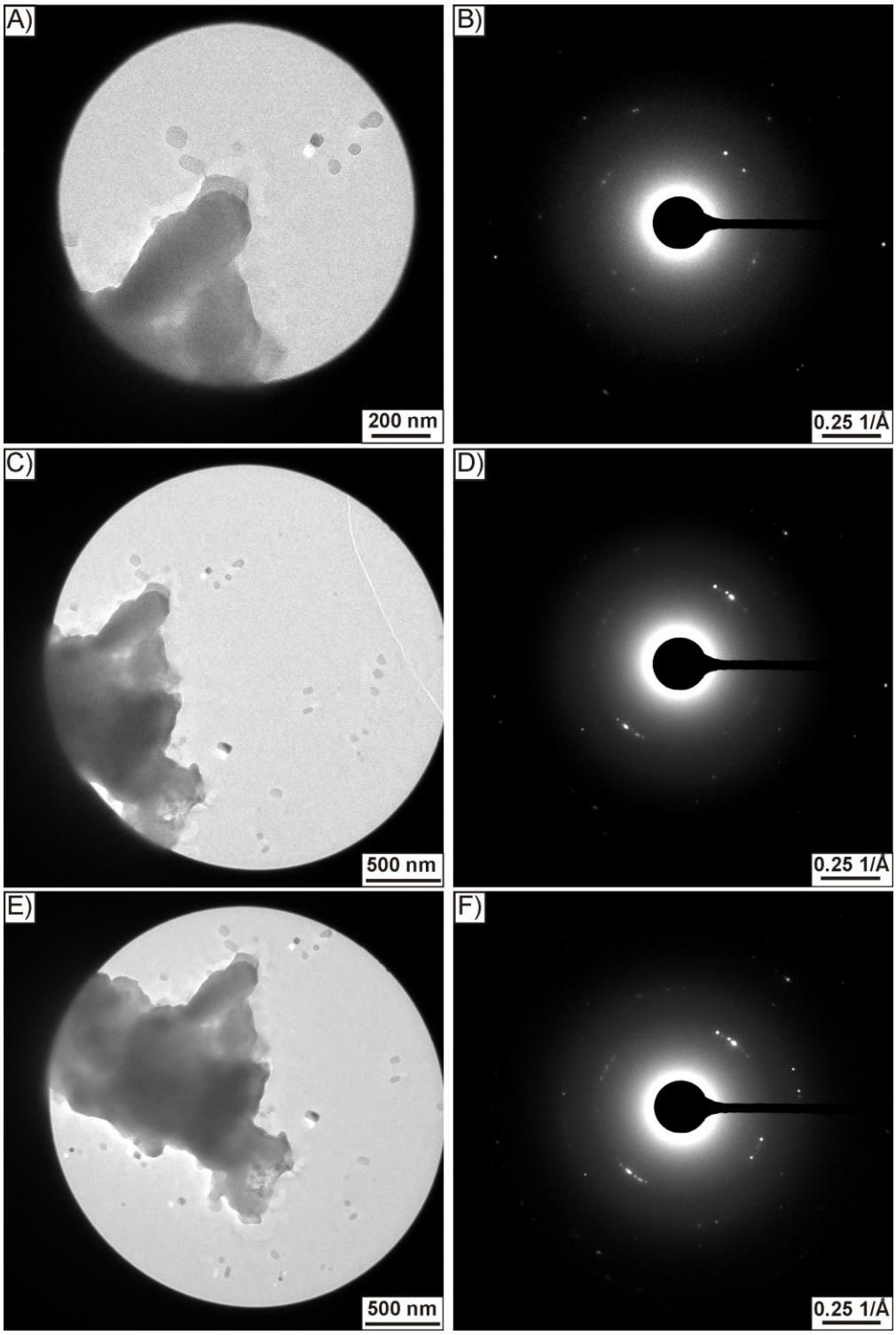

fig. S5. Evaluation of the mesocrystalline domain sizes of self-assembled C-S-H crystals (approach A). Left side: diffraction area; **right side:** corresponding diffraction patterns. Single crystalline scattering behavior can be observed for an area as large as approximately 1 μm². With bigger diffraction areas the spot-like pattern transfers into arcs, indicating the transition to a polycrystalline material.

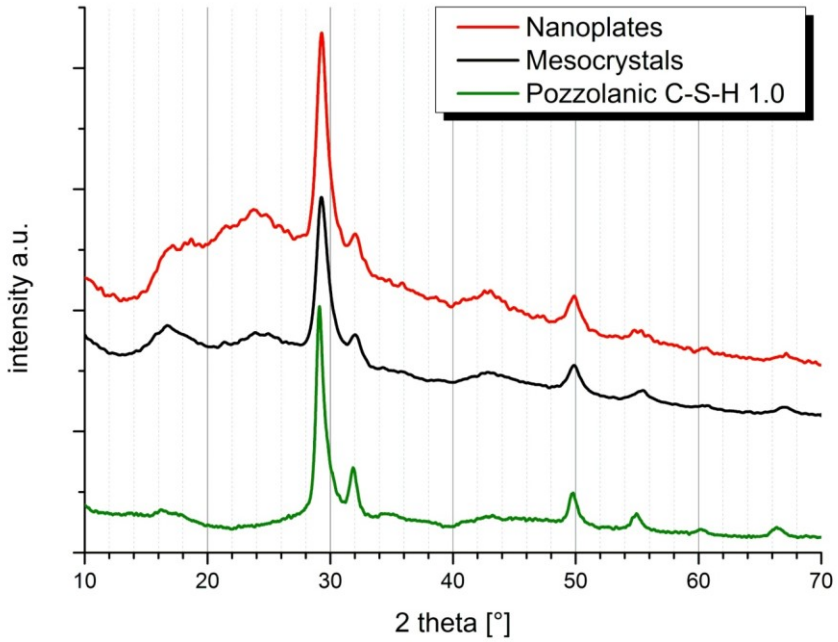

fig. S6. Wide-angle x-ray pattern of filtered polymer-stabilized C-S-H nanoplates (red curve) and obtained mesocrystals from pH increase (approach A, black curve) compared to C-S-H from pozzolanic reaction with CaO and SiO2 (Ca/Si = 1) (green curve). They are all similar to patterns of fully hydrated cement paste made with alite or belite *(36*, *49)*. Due to the smaller amount of material the nanoplates give more noisy signals. However, the spectra are qualitatively equal so that every peak can be assigned to C-S-H. The not existent peak sharpening for the black curve indicates that the mesocrystals are made out of single C-S-H crystallites, which are not fused together.

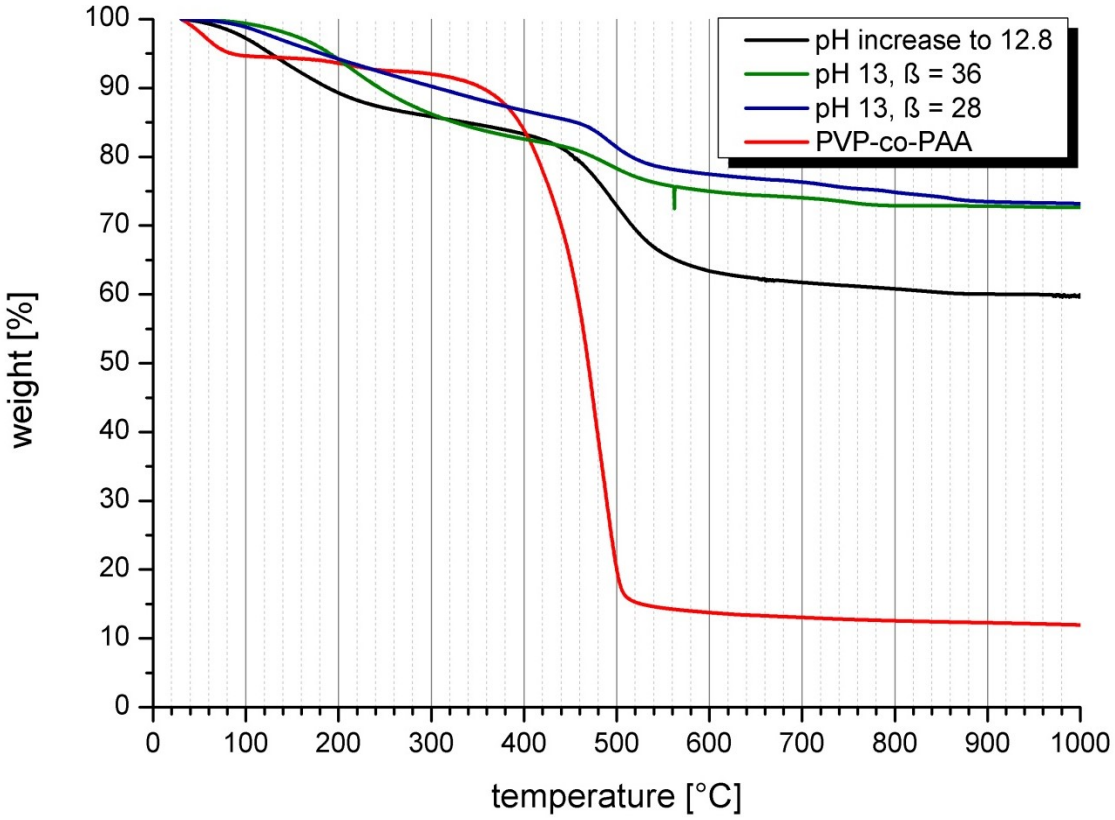

fig. S7. Thermogravimetric analysis of C-S-H mesocrystals. a) pH increase of colloidal C-S-H to 12.8 (black curve, approach A) and b) supersaturation of a Na_2SiO_3 solution at pH 13 with calcium (approach B) to supersaturation values of ß = 28 (blue curve) and ß = 36 (green curve). Data suggest an organic content of the mesocrystals between 5 and 20 wt. %. The decomposition curve of the pure polymer (PVP-co-PAA, red curve) is given for comparison.

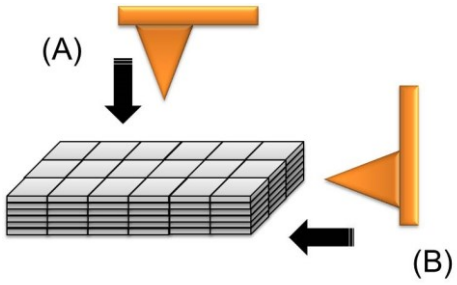

fig. S8. Schematical illustration of the two differently performed nanoindentation experiments on C-S-H mesocrystals from approach A. (A) Nanoindentation perpendicular to the layered structure: reduced modulus: 10.4 ± 1.8 GPa; hardness: 0.45 ± 0.14 GPa. **(B)** Nanoindentation parallel to the layered structure: reduced modulus: 9.8 ± 1.4 GPa; hardness: 0.40 ± 0.07 GPa.

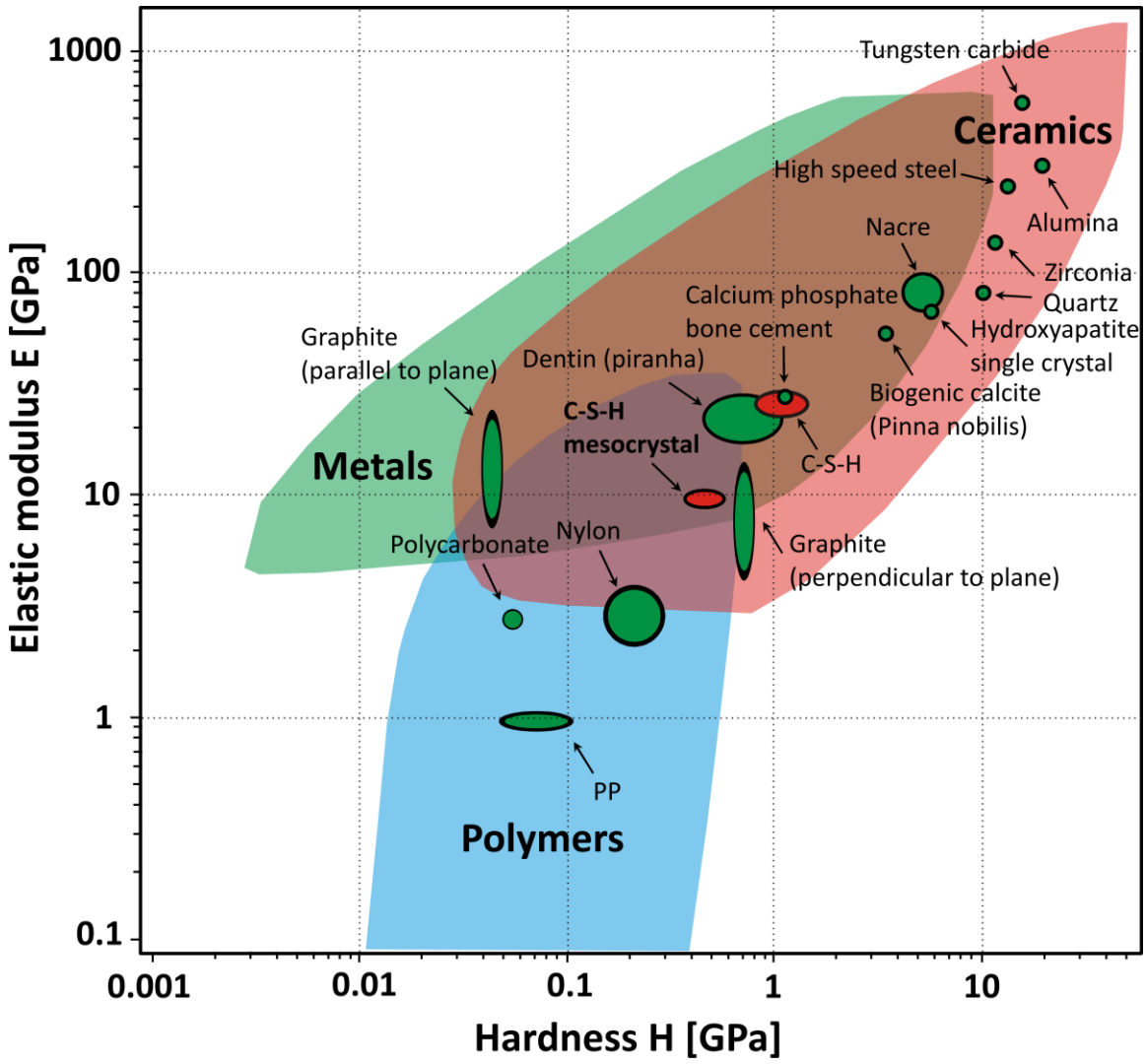

fig. S9. Ashby plot comparing the mechanical properties of the C-S-H mesocrystals (approach A) with various materials.

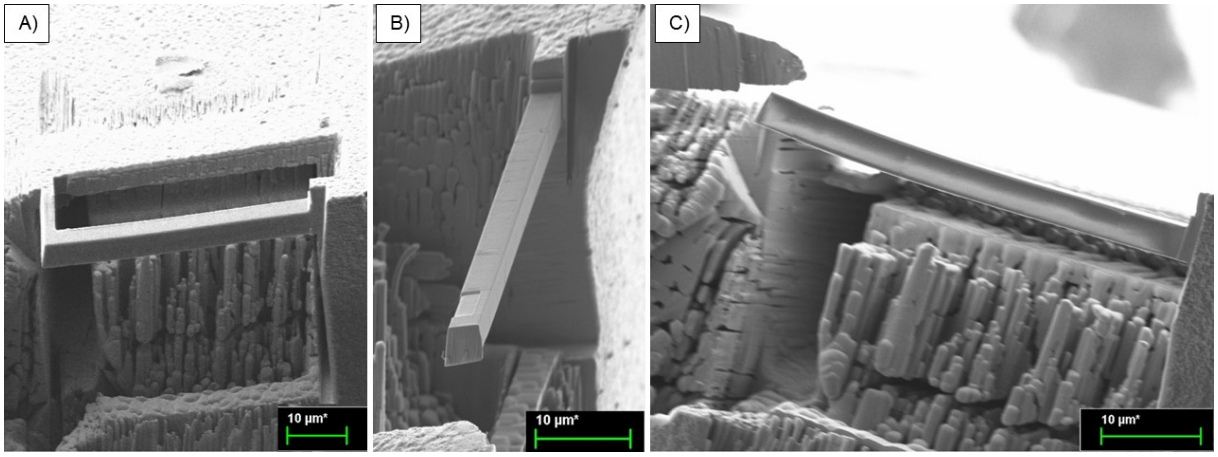

fig. S10. SEM images of a cantilever beam used in the bending tests with the applied load perpendicular to the crystal layer planes. A) Before the last cutting step, B) after the last cutting step yielding the cantilever beam clamped on one end, C) snap shot of the experimental configuration, the load is applied using the tip of the tungsten needle of the manipulator.

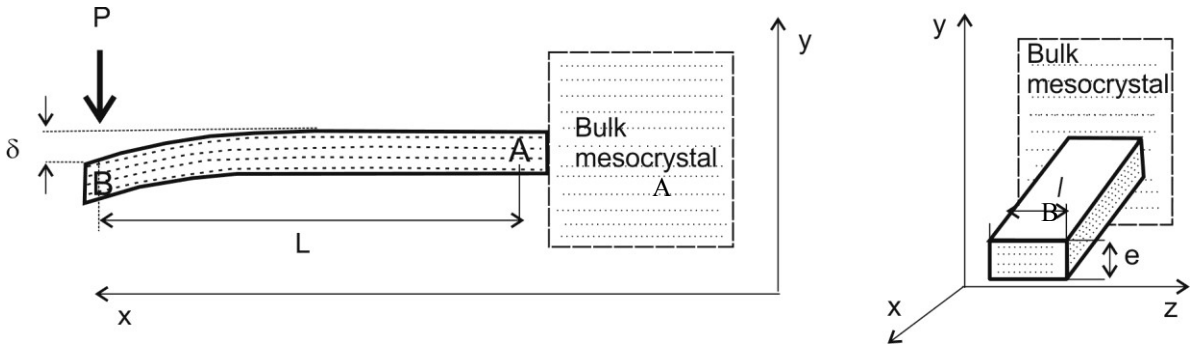

fig. S11. Schematic illustration of in-situ bending experiments. Schematic illustration of the mechanical deformation of the cantilever beam by applying a load P at point B (left) and cantilever dimensions (right). Adapted from Ref. *(46)*.

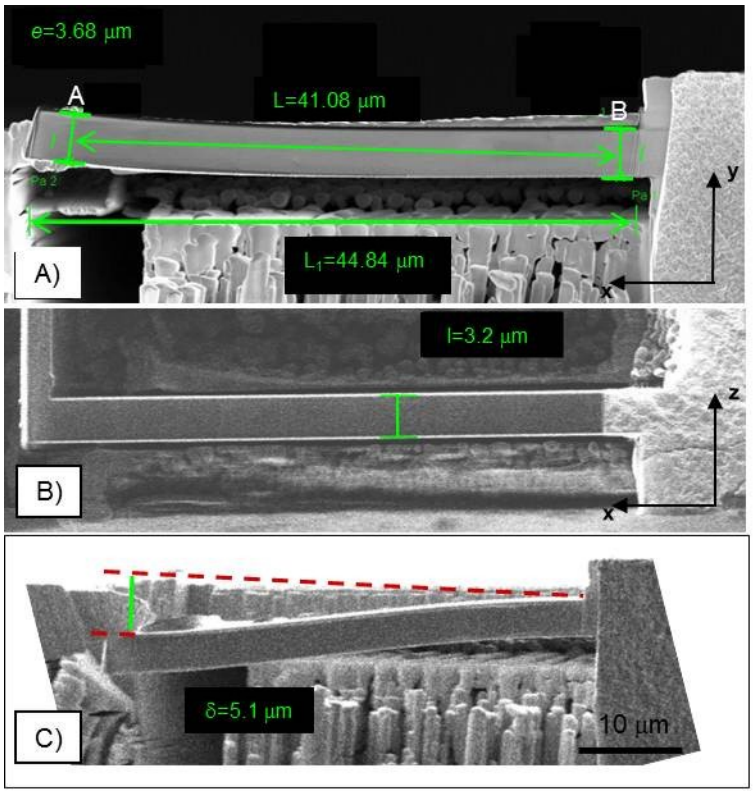

fig. S12. Dimensions of a cantilever beam used in the bending tests with the load applied perpendicular to the crystal layers. A, B, C images are different views of the cantilever where dimensions of the cantilever beam, used for calculating the load and maximal bending stresses, are shown. e, l, L_1, L, and δ are the cantilever's thickness, width, length, distance between the points A and B, and displacement upon application of the load, respectively. The corresponding video is provided as movie S1.

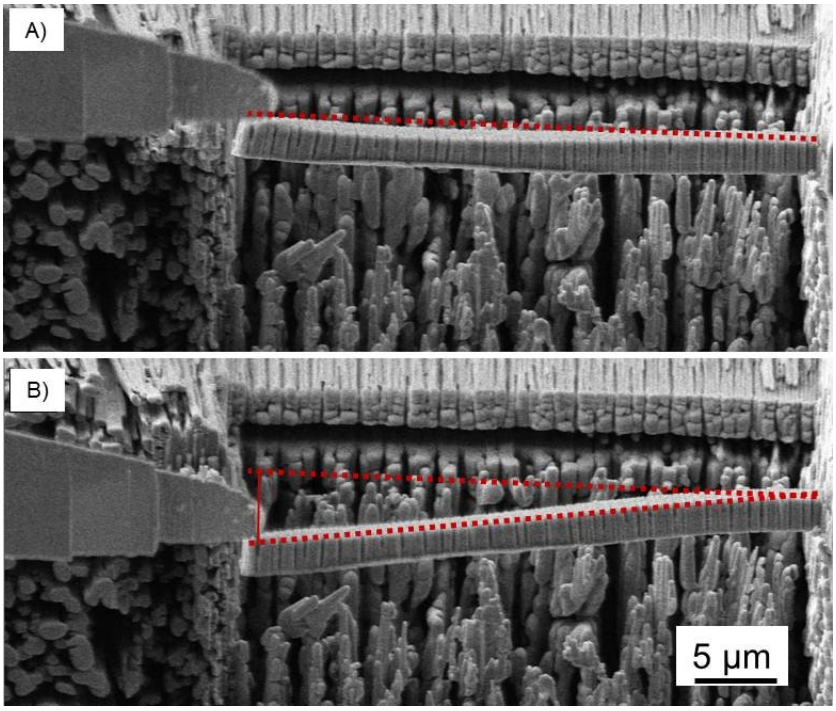

fig. S13. SEM images of a cantilever beam used in the bending tests with the load applied parallel to the crystal layers. A) snap shot of the initial stage, B) cantilever bending upon applying load by the tip of the tungsten needle of the manipulator. The flexural stress calculated for the load applied parallel to the crystal layer planes was estimated to be 162 MPa. The corresponding video is provided as movie S2.

Supplementary Movie legends

movie S1. Bending test of mesocrystals obtained from pH increase to pH 12.8 under the scanning electron microscope. The flexibility of C-S-H mesocrystals can be clearly seen as the sample can be bent under mechanical stress and bends back when stress is released. Moreover, the C-S-H mesocrystal does not break.

movie S2. Bending test of the same mesocrystals such as in movie S1 except that the applied stress is parallel to the crystal layer planes.